Organic Electronics 13 (2012) 870–874

Contents lists available at SciVerse ScienceDirect

Organic Electronics

journal homepage: www.elsevier.com/locate/orgel

Letter

Zinc Tin Oxide (ZTO) electron transporting buffer layer in inverted organic solar cell

Than Zaw Oo [a], R. Devi Chandra [b], Natalia Yantara [a], Rajiv Ramanujam Prabhakar [b], Lydia H. Wong [a], Nripan Mathews [a,b,*], Subodh G. Mhaisalkar [a,b]

[a] School of Materials Science and Engineering, Nanyang Technological University, Singapore 639798, Singapore
[b] Energy Research Institute @ NTU (ERI@N), Singapore 637553, Singapore

ARTICLE INFO

Article history:
Received 1 August 2011
Received in revised form 30 December 2011
Accepted 15 January 2012
Available online 31 January 2012

Keywords:
Electron transporting layer
Zinc Tin Oxide
High electron mobility
Inverted organic solar cell
Power conversion efficiency

ABSTRACT

Solution processed, high electron mobility and highly transparent Zinc Tin Oxide (ZTO) was successfully exploited as electron transporting buffer layer in an inverted organic solar cell. The device configuration of FTO/ZTO/P3HT:PCBM/WO_3/Ag was employed. For comparison, an identical device using a sol–gel derived TiO_x electron extracting layer was also fabricated. Increased short-circuit density (J_{sc}) and open-circuit voltage (V_{oc}) were generated in the devices with ZTO layer in comparison to the ones with TiO_x layer. It is attributed to a better electron transporting, hole blocking capacities and reduced recombination probabilities at electron collecting electrode with ZTO layer. A power conversion efficiency of 3.05% was achieved with ZTO devices.

1. Introduction

Organic photovoltaic (OPV) cells have attracted much attention due to their ease of processing, low cost and the possibility of fabricating large area flexible devices. The power conversion efficiency of OPV devices have reached 7–8% due to the continued development of low band gap polymers and control over active layer morphology. The conventional device structure for these solar cells utilizes indium tin oxide (ITO) coated with poly(3,4-ethylene dioxythiophene):(polystyrene sulfonic acid) (PEDOT:PSS) as an anode and aluminum as a cathode [1,2]. This standard architecture generally leads to inherent device instability due to the oxidization of low work function electrodes (Al and Ca/Al) and the degradation of ITO by the strong acidity of PEDOT:PSS [3]. This instability can be improved by alternative device geometries such as the inverted structure which include reversed polarities of electrodes and the addition of carrier selective anodic/cathodic metal oxide buffers. In inverted device configuration, cathodic buffer layers (TiO_2 and ZnO) and anodic buffers (MoO_3 and WO_3) have been integrated for improved electron and hole transport, respectively [3–8]. A transparent conducting ITO is still used on the light-illuminated side, but in cases which demand high temperature annealing, the optical transmission and work function of ITO can fluctuate, affecting device performance [9]. Rather, fluorine-doped tin oxide (FTO) can be utilized because it is thermally and chemically more stable than ITO [10].

As mentioned earlier, the commonly used *n*-type metal oxides for cathode interface modification in organic photovoltaic cells are TiO_2 and ZnO. In addition, Titanium suboxide (TiO_x) has been shown to be a very good cathode buffer layer enabling 50% efficiency enhancement in organic solar cells [11]. These electron transport materials facilitate a better alignment between the LUMO of PCBM and the work function of electron collecting electrode. Moreover, their deeper valence band edge prevents the flow of holes in undesirable direction. In previously reported inverted solar cells, a wide range of power conversion efficiencies

* Corresponding author at: School of Materials Science and Engineering, Nanyang Technological University, Singapore 639798, Singapore.
E-mail address: Nripan@ntu.edu.sg (N. Mathews).

1566-1199/$ - see front matter © 2012 Elsevier B.V. All rights reserved.
doi:10.1016/j.orgel.2012.01.011

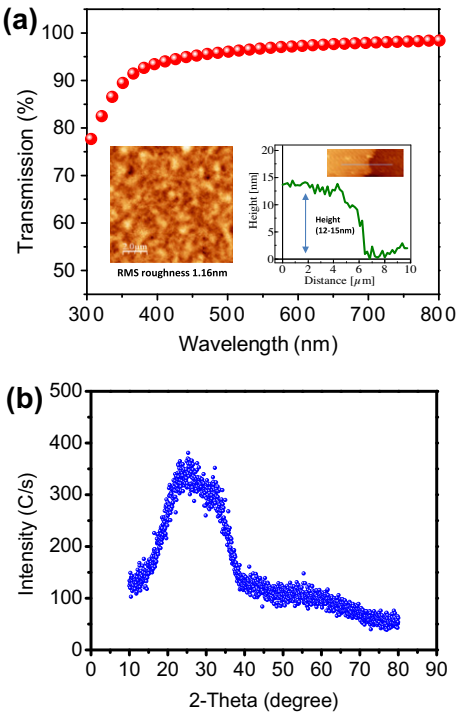

Fig. 1. (a) Transmission spectrum and (b) XRD pattern of ZTO film. Insets in (a) are AFM Surface topography image and its step height profile of ZTO film on quartz substrate.

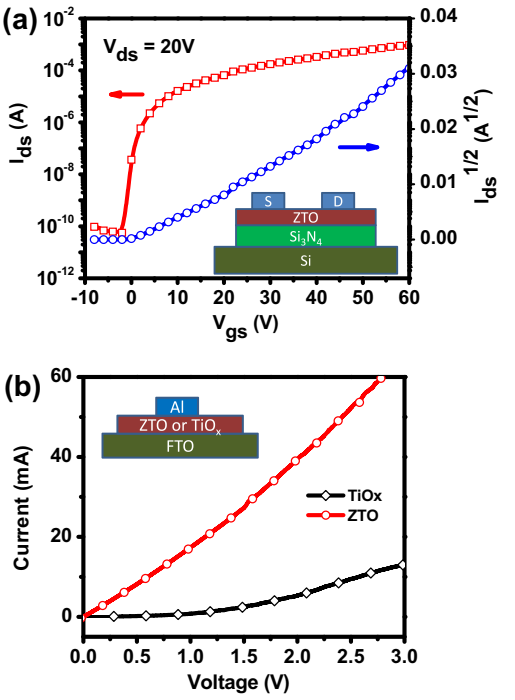

Fig. 2. (a) Drain current versus gate voltage (I_{ds}–V_{gs}) and the square root of the drain current versus gate voltage ($\sqrt{I_{ds}} - V_{gs}$) transfer characteristics of the ZTO thin film transistor. (b) Current–voltage characteristics of ZTO and TiO_x films obtained from two-terminal configuration.

have been generated depending on the weight blend ratio of donor–acceptor materials, thickness and annealing temperature of photoactive layer, electron and hole transporting buffers, electrode materials, etc. [5–8]. A PCE of 4% was achieved in an optimized inverted solar cell with ZnO nanoparticles as electron transport layer [8] while PCE of 2.1% with electrodeposited amorphous TiO_x [7].

In addition to ZnO and TiO_x, amorphous Zinc Tin Oxide (ZTO) is found to be a promising *n*-type metal oxide that has been demonstrated as the channel material in thin film transistors. The field effect electron mobility of ZTO prepared by RF magnetron sputtering and post-annealed at 600 °C is as high as 20–50 cm^2/V s [12]. Instead of traditional vacuum deposition techniques such as pulse laser deposition and RF magnetron sputtering, solution-processed deposition techniques such as spin coating, dip coating and inkjet printing will add the advantage of reduced manufacturing cost, high throughput, large area coverage and the direct writing capabilities from inkjet printing. Solution processed amorphous ZTO would be an interesting low-cost material for flexible electronics and photovoltaic applications. To the best of our knowledge, solution processed ZTO films have not yet been employed as electron transport layer in photovoltaic application. In this letter, we have exploited a solution processed, high electron mobility and highly transparent ZTO film as an electron transporting buffer layer in an inverted OPV cell. An inverted cell configuration (FTO/ZTO/P3HT:PCBM/WO_3/Ag) was employed. For comparison, an identical device with the TiO_x buffer layer instead was also fabricated.

2. Materials and methods

The precursor solution for fabrication of ZTO film was prepared by dissolving equal molar ratios of $ZnCl_2$ and $SnCl_2$ (0.07 M) in acetonitrile solvent. The solution was spin coated on quartz substrates followed by annealing at 100 °C for 1hr and at 500 °C for 1 h to form the ZTO films [13]. The optical, morphological and structural properties of ZTO film were characterized by UV–Vis spectrophotometer (Shimadzu UV-3600), Atomic Force Microscopy (Asylum Research MFP-3D stand-alone) and X-ray Diffraction (Bruker D8 Advance), respectively. The inverted OPV cells with an electron transporting ZTO layer were fabricated on FTO coated glass substrates. The FTO coated glasses were cleaned with detergent, de-ionized water and ethanol followed by oxygen plasma treatment for 10 min. They were then treated with 1 M NaOH solution to make it hydrophilic. For electron transporting layer, the ZTO solution prepared as mentioned above was spin coated on FTO glass. For reference device, TiO_x sol–gel was prepared following literature procedures [11] and spin-coated on FTO coated glass. The thickness of the resulting ZTO and TiO_x films are 10–15 nm as measured by atomic force microscopy (AFM) step-height profile. Then the ZTO and TiO_x coated FTO substrates were transferred into nitrogen glove box to deposit the photoactive BHJ layers. A mixed solution of Poly(3-hexylthiophene-2,5-diyl): [6,6]-phenyl C_{60}-butyric acid methyl ester (P3HT:PCBM) (1:0.8) in dichlorobenzene (DCB) with concentration of 20 mg/ml was spin-coated on these films.

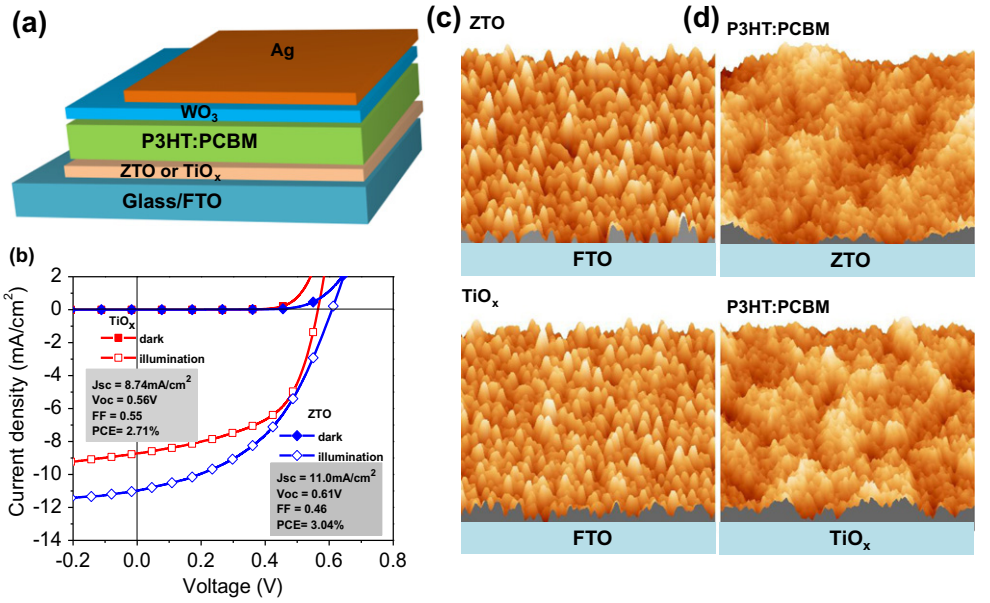

Fig. 3. (a) Schematic structure of inverted solar cell with photoactive layer (P3HT:PCBM), electron selective layer (ZTO or TiO_x) and hole selective layer (WO_3). (b) Current–voltage characteristics of the devices along with the corresponding the device parameters. (c) AFM topography images (5 × 5 μm) of ZTO and TiO_x on FTO substrate having RMS roughness of 10.44 nm and 14.29 nm. (Note: RMS roughness of FTO is 14.34 nm). (d) AFM topography images (5 × 5 μm) of P3HT:PCBM film on top of ZTO and TiO_x having RMS roughness of 1.35 nm and 1.15 nm, respectively.

The thicknesses of active layers are 170 nm measured by surface profilometry (Alpha-Step-IQ). The photoactive film was annealed at 150 °C for 10 min prior to deposition of hole transporting layer WO_3 (10 nm) and hole collecting electrode Ag (100 nm) by thermal evaporation. The effective cell area defined by the geometrical overlap between ITO and Al is 0.071 cm^2. The current–voltage characteristic of the devices in dark and under illumination was recorded with an HP 4155 semiconductor analyzer. The cells were then illuminated by an Air Mass 1.5 Global (AM 1.5 G) solar simulator (San-Ei XES-300, AAA rating) with an irradiation intensity of 1000 W/m^2. The testing for all devices was performed in an inert nitrogen atmosphere.

3. Results and discussion

Fig. 1 a shows the transmission spectra of ZTO film on quartz indicating that the ZTO film is highly transparent with T% of ~95% in the visible region (400–800 nm). The band gap calculated from the plot of $(\alpha h\nu)^2$ versus hv is 3.6 eV, consistent with previous reports on the ZTO band gap of 3.35–3.89 eV [12,14]. The AFM height image profile (inset of Fig. 1a) shows that the thickness of ZTO film is 12–15 nm. The surface topography image of ZTO film on quartz substrate (inset of Fig. 1a) reveals that the surface of the film is smooth and RMS roughness was 1.16 nm. The X-ray diffraction (XRD) profile (Fig. 1b) confirms the amorphous nature of the ZTO film.

The field effect mobility of a material reflects the current driving capacity that in turn is determined by the charge transport properties of that material. Thus, the field effect mobility of ZTO film was evaluated by fabricating field effect transistors (FET) with ZTO as channel material. Here, we fabricated the ZTO FET using a bottom-gate test structure (Inset of Fig. 2a). The ZTO film was deposited on the Si_3N_4 dielectric (200 nm) coated Si substrate followed by optimized annealing at 100 °C for 1hr and 500 °C for 1hr. The aluminum was deposited through patterned mask on top to ZTO as source and drain electrodes. The channel mobility of ZTO was extracted from slope of $\sqrt{I_{ds}}$ versus V_{gs} in the transfer characteristics (Fig. 2a) and was as high as 3.21 $cm^2/V\,s$, when measured in vacuum and 2.55 $cm^2/V\,s$ in air. The drain current ON/OFF ratio was 10^6 in the V_{gs} range of −10 V to 60 V. The mobility of ZTO is found to be significantly higher than that of TiO_x (1.7×10^{-4} $cm^2/V\,s$) [11,15], although it is to be noted that the TiO_x mobility was measured through time of flight method. The high mobility displayed by amorphous ZTO is due to its high ionicity. The conduction band minimum (CBM) and valance band maximum (VBM) are formed from different ionic states. The CBM of oxides made up of spherically expanded s-orbitals which overlap with s-orbitals of neighboring metals. So electronic levels of CBM are not altered by strained bonds and the electron transport is not affected significantly [16].

A parameter which determines the performance of the electron transport layer in the solar cell is its conductivity, which determines the voltage drop across the layer. Thus, the electrical conductivities of ZTO as well as TiO_x films were also measured by two-terminal configuration (FTO/ZTO or TiO_x/Al) (inset of Fig. 2b). The films were spun-coat on FTO followed by Al deposition, the same condition as in the solar cell structure. Fig. 2(b) shows the current–voltage (I–V) characteristics of ZTO and TiO_x films. The electrical conductivities of ZTO and TiO_x as determined from their I–V curves are 1.10×10^{-4} $S\,m^{-1}$ and 2.37×10^{-5} $S\,m^{-1}$,

respectively. The conductivity of ZTO is about an order of magnitude higher than that of TiO_x – indicating that the ZTO film could be applied as an electron transport layer in inverted solar cells. Additionally, the wettability of ZTO and TiO_x underlying layers towards subsequent deposition of P3HT:PCBM blend film were studied by the contact angle measurement as the surfaces of polar hydrophilic oxides are often chemically incompatible with non-polar organic films leading to delamination of organic film [17] and increasing the contact resistance. Similar contact angles (11.5° with ZTO and 9.8° with TiO_x) indicated that wettability is not a significant concern.

Fig. 3(a) shows the device configuration of the inverted solar cell. In contrast to conventional solar cells, electron collection occurs at the transparent conducting oxide (FTO in this case) while hole collection is performed at the Ag electrode. Thus the role of electron and hole buffer layers in selectively allowing transport of one type of carrier while blocking the other is very critical. The current–voltage characteristics in dark and under illumination of the devices with ZTO and TiO_x electron transport layers are depicted in Fig. 3(b) along with the corresponding device parameters. Power conversion efficiencies of 3.04% and 2.71% were achieved in the devices with ZTO and TiO_x, respectively. A similar device configuration (FTO/TiO_x/P3HT:PCBM/PEDOT:PSS/Au) was reported by Kuwabara et. al. with a PCE of 2.13% (J_{sc} 6.95 mA/cm^2, V_{oc} 0.55, FF 0.56) [7]. Although our devices showed the same V_{oc} and FF as Kuwabara et al. our TiO_x devices displayed higher J_{sc}. An increased J_{sc} in our device is likely due to better electron and hole transport properties with spin-coated sol–gel based TiO_x and WO_3 rather than electrodeposited TiO_x and PEDOT:PSS. Thus an enhanced device performance can be achieved through careful selection of electron and hole extracting layers in devices. With ZTO layer, a further enhancement of the device efficiency was obtained, mainly deriving from increased V_{oc} and J_{sc}.

The inverted solar cell with ZTO layer gives the open circuit voltage (V_{oc}) of 0.61 V and short circuit current density (J_{sc}) of 11.0 mA/cm^2 higher than V_{oc} of 0.56 V and J_{sc} of 8.74 mA/cm^2 with TiO_x layer. It is attributable to better charge transport and collection properties. As the charge transport/collection at electrode is influenced by the mobility of charge extracting layers, the high electron mobility of ZTO allows the efficient electron transport/collection at the electrode, thereby reducing charge recombination. In addition, as ZTO and TiO_x materials act as both electron transporting and hole blocking layers between photoactive materials and FTO electrode, they should completely cover the FTO substrate. But it is hard to have a complete coverage on FTO because FTO roughness is very high (RMS roughness 14.34 nm, data not shown). The statistical evaluation on atomic force microscopy (AFM) height images (Fig. 3c and d) shows that RMS roughness of ZTO and TiO_x on FTO is 10.44 nm and 14.29 nm, respectively. A reduced roughness with ZTO layer implies the better coverage of ZTO on FTO substrate that will enable effective blocking of the photogenerated holes. Hence, ZTO buffer with better electron transporting, hole blocking capacities and reduced recombination probabilities at electron collecting electrode results in enhanced V_{oc} and J_{sc} in the device with ZTO layer.

Despite the increased V_{oc} and J_{sc} with ZTO layer, the FF was lower in the device with ZTO (0.46 with ZTO and 0.55 with TiO_x). The fill factor (FF) of the device is sensitive to the series resistance of the device and the morphology of the photoactive film [18–20]. The surface morphologies of P3HT:PCBM films on ZTO and TiO_x are similar and about 1.35 nm and 1.15 nm, respectively (Fig. 3c and d). The series resistances of the devices were extracted from the inverse derivative of current with respect to voltage in current–voltage curve around the open-circuit point. The calculated R_s of the devices with ZTO and TiO_x are 19.68 Ω cm^2 and 11.92 Ω cm^2, respectively. The series resistance extracted from the solar cell is determined by the conductivity of all the layers within the solar cell as well as the contact resistances at each electrode. In the case where we are comparing different electron transport layer (ZTO vs TiO_x) integrated devices, the primary differences stem from the alignment of active layer energy levels with that of the electron transport layer, the conductivity of the electron transport layer as well as its own energy level alignment with the transparent electrode (FTO). In addition, the difference in resistance can come from different surface areas of the contacts. A surface analysis on AFM topography images (5×5 μm- Fig. 3(c)) using Igor Pro 6.12A software provides the surface areas of 25.9 μm^2 and 27.0 μm^2 and the corresponding area percents of 3.77% and 8.02%, respectively for ZTO and TiO_x interlayer on FTO substrates. This difference is again not significant to explain the differences in the series resistance. Since our measurements seem to indicate that the conductivity of ZTO is superior to that of TiO_x, the difference in the series resistance could stem from misalignment at the active layer/ZTO interface or the FTO/ZTO interface.

4. Summary

In summary, we prepared *n*-type ZTO film by a solution-processed method. It is amorphous in nature and its transmission is higher than 95% in visible region. The field effect mobility is as high as 3.21 cm^2/V s measured by ZTO thin film transistor with bottom-gate structure. In addition, the electrical conductivity of ZTO measured by two-terminal diode configuration is 1.10×10^{-4} S m^{-1}, higher than that of TiO_x. We demonstrated an inverted organic solar cell exploiting ZTO film as an efficient electron extracting layer and power conversion efficiency is as high as 3.05%. As compared to the device with TiO_x layer, the enhanced device efficiency with ZTO mainly derives from higher J_{sc} and V_{oc}. Thus, the good electron transport properties and transparency of the ZTO layer demonstrates its potential as electron buffer layer in organic solar cells.

References

[1] J.Y. Kim et al., Efficient tandem polymer solar cells fabricated by all-solution processing, Science 317 (2007) 222–225.
[2] Y. Liang et al., For the bright future – bulk heterojunction polymer solar cells with power conversion efficiency of 7.4%, Advanced Materials 22 (2010) E135–E138.
[3] S.K. Hau et al., A review on the development of the inverted polymer solar cell architecture, Polymer Reviews 50 (2010) 474–510.

[4] S.K. Hau et al., Air-stable inverted flexible polymer solar cells using zinc oxide nanoparticles as an electron selective layer, Applied Physics Letters 92 (2008) 253301.
[5] R. Steim et al., Interface modification for highly efficient organic photovoltaics, Applied Physics Letters 92 (2008) 093303.
[6] H. Schmidt et al., Efficient semitransparent inverted organic solar cells with indium tin oxide top electrode, Applied Physics Letters 94 (2009) 243302.
[7] T. Kuwabara et al., Inverted type bulk-heterojunction organic solar cell using electrodeposited titanium oxide thin films as electron collector electrode, Thin Solid Films 517 (2009) 3766–3769.
[8] S.K. Hau et al., High performance ambient processed inverted polymer solar cells through interfacial modification with a fullerene self-assembled monolayer, Applied Physics Letters 93 (2008) 233304.
[9] Y. Yan et al., Structural instability of Sn-doped In2O3 thin films during thermal annealing at low temperature, Thin Solid Films 515 (2007) 6686–6690.
[10] J.-R. Kim et al., Improvement of the performance of inverted polymer solar cells with a fluorine-doped tin oxide electrode, Current Applied Physics 11 (2011) S175–S178.
[11] J.Y. Kim et al., New architecture for high-efficiency polymer photovoltaic cells using solution-based titanium oxide as an optical spacer, Advanced Materials 18 (2006) 572–576.
[12] H.Q. Chiang et al., High mobility transparent thin-film transistors with amorphous Zinc Tin Oxide channel layer, Applied Physics Letters 86 (2005) 013503.
[13] C.G. Lee, A. Dodabalapur, Solution-processed zinc-tin oxide thin-film transistors with low interfacial trap density and improved performance, Applied Physics Letters 96 (2010).
[14] D. Kim et al., Inkjet-printed Zinc Tin Oxide thin-film transistor, Langmuir 25 (2009) 11149–11154.
[15] L.-M. Chen et al., Interface investigation and engineering – achieving high performance polymer photovoltaic devices, Journal of Materials Chemistry 20 (2010) 2575–2598.
[16] T. Kamiya et al., Origins of high mobility and low operation voltage of amorphous oxide tfts: electronic structure, electron transport, defects and doping*, Journal of Display Technology 5 (2009) 468–483.
[17] J.S. Kim et al., Surface energy and polarity of treated indium–tin–oxide anodes for polymer light-emitting diodes studied by contact-angle measurements, Journal of Applied Physics 86 (1999) 2774–2778.
[18] T.Z. Oo et al., Investigation of photophysical, morphological and photovoltaic behavior of poly(p-phenylene vinylene) based polymer/oligomer blends, Thin Solid Films 518 (2010) 5292–5299.
[19] M.-S. Kim et al., Effective variables to control the fill factor of organic photovoltaic cells, ACS Applied Materials & Interfaces 1 (2009) 1264–1269.
[20] V. Djara, J.C. Bernède, Effect of the interface morphology on the fill factor of plastic solar cells, Thin Solid Films 493 (2005) 273–277.